

## Cross sections and ion kinetic energies for electron impact ionization of CH<sub>4</sub>

K. Gluch<sup>1</sup>, P. Scheier, W. Schustereder, T. Tepnual, L. Feketeova,  
C. Mair, S. Matt-Leubner, A. Stamatovic<sup>2</sup>, T. D. Märk\*

*Institut für Ionenphysik, Leopold-Franzens Universität Innsbruck, Technikerstr. 25, A-6020 Innsbruck, Austria*

Received 8 January 2003; accepted 17 March 2003

### Abstract

Total and partial cross sections for electron impact ionization of CH<sub>4</sub> were measured from threshold to 1000 eV. Ion kinetic energy distributions were measured applying a deflection and retarding field method. The extraction of ions from the ion source was simulated fully three-dimensionally including the presence of a magnetic field for electron guidance. Thereby, discrimination factors were determined as a function of the initial ion kinetic energy. Multiplication of these factors with the ion signal leads to relative partial cross sections. By normalizing the sum of these partial cross sections to an absolute value taken from the literature, absolute partial cross sections were obtained that agree well with previous measurements where a complete collection of the product ions has been demonstrated. Moreover, with the present method, it is possible to determine cross sections that are differential with respect to the initial kinetic energy of the ion.

© 2003 Elsevier Science B.V. All rights reserved.

*Keywords:* Cross sections; Ion kinetic energy; Electron impact ionization; CH<sub>4</sub>

### 1. Introduction

Dissociative ionization of molecules induced by electron impact is a very important process in many different areas such as low-temperature plasmas, radiation chemistry, edge plasmas in fusion reactors, mass spectrometry, and chemical analysis [1–5]. Ionic and

neutral fragments produced via dissociative ionization often carry substantial amounts of kinetic energy, and the kinetic energy distribution of a particular fragment determines the energy deposition and the energy transfer pathways in the corresponding media. Thus, the modeling of environments where dissociative ionization processes are important requires knowledge not only of the production efficiency and the nature of fragment ions produced but also of their kinetic energy distribution. Furthermore, different pathways leading to the formation of the same fragment ion may have different threshold energies and different exothermicities. Thus, the kinetic energy distribution for a given fragment ion can depend strongly on the electron energy.

\* Corresponding author. Also adjunct professor at Department of Plasmaphysics, Comenius University, SK-84248 Bratislava, Slovak Republic.

*E-mail address:* [tilmann.maerk@uibk.ac.at](mailto:tilmann.maerk@uibk.ac.at) (T.D. Märk).

<sup>1</sup> Present address: Department of Physics, Mathematics and Informatics, University Marie Curie Skłodowskiej, Lublin, Poland.

<sup>2</sup> Present address: Faculty of Physics, P.O. Box 638, Yu-11001 Beograd, Yugoslavia.

Fragment ions that are formed with high kinetic energies often are collected with considerably reduced efficiency which has a strong influence on the cross section values determined [6–9]. With specially dedicated instruments that were constructed to assure uniform collection efficiency absolute partial and total cross sections have been measured [10,11]. However, with commercial instruments, comparable results can only be obtained if the discrimination factor for high energetic fragment ions is determined. For a standard double focusing mass spectrometer equipped with a modified Nier-type ion source, Poll et al. [6] demonstrated that ion trajectory calculations of the extraction region of this ion source allows the determination of the corresponding ion loss. After correction of the ion efficiency curves with these discrimination factors the agreement with the above mentioned data from the specially dedicated instruments is extremely good. In order to get information on the kinetic energy of the ions, a deflection method was applied in the direction perpendicular to the plane of the mass spectrometer. The present work is an extension of this method and in contrast to Poll et al. [6] the kinetic energy distribution of the fragment ions is used to determine for the first time ion kinetic energy differential cross sections for these fragment ions. Furthermore, highly energetic ions like  $\text{H}^+$  and  $\text{H}_2^+$  were measured too, which was not possible in the study of Poll et al. [6]. The determination of the kinetic energy distributions of the fragment ions as a function of the electron energy allows to distinguish between different ionization processes that lead to the production of a given fragment ion [12,13]. Hydrocarbon molecules are known to form fragment ions with broad kinetic energy distributions ranging from thermal energies to many electronvolts [6,12,14–16]. This is especially true for light fragment ions such as  $\text{H}^+$  and  $\text{H}_2^+$  as a result of the momentum conservation. In some cases, such as, for instance, propane, many of the energetic ions are formed with higher probabilities than the thermal ions (see e.g., Poll et al. [6] and references cited therein).

Hydrocarbon molecules are abundant constituents of planetary atmospheres and major compounds in combustible gas mixtures and in fusion edge plasmas

[1–5]. Methane is the simplest of these hydrocarbon molecules. Thus, absolute total and partial photon [17–19] and electron [20–25] ionization cross sections and nascent fragment ion energy distributions [12,13,26–28] have been studied extensively for this molecule. For the deuterated methane molecule electron impact ionization and dissociative ionization cross sections were determined for the  $\text{CD}_x$  ( $x = 1–4$ ) molecule and radicals applying a fast neutral beam technique [29]. Electron impact total ionization cross sections have been determined also theoretically applying the BEB (Binary-Encounter-Bethe) model [30], the DM (Deutsch–Märk) method [31], and the JK (Jain–Khare) method [32]. Partial electron impact ionization cross sections were calculated for methane [33,34] as well as total electron impact cross sections for various  $\text{CH}_x$  radicals [35].

All previous studies [12,13,27,36–38] found that essentially all fragment ions of methane are formed with complex energy distributions with two major components, a low-energy component comprised of thermal and/or quasi-thermal (“slow”) ions with maximum kinetic energies of  $\sim 0.3$  eV and energetic (“fast”) ions with a broad energy distribution from 0.5 to  $\sim 10$  eV. It has been suggested that several dissociation pathways contribute to the formation of the various fragment ions, as demonstrated by the different appearance energies that were measured for the respective slow and fast component in the kinetic energy distribution of a given fragment ion [13,38].

## 2. Experimental

The presently used apparatus is a double focusing Nier–Johnson two-sector-field mass spectrometer of reversed geometry with a Nier-type electron impact ion source and has been described in detail in earlier publications [6,16,39,40]. Fig. 1 shows the experimental setup schematically. Stagnant target gas is crossed by a well-characterized magnetically collimated electron beam with an FWHM energy spread of  $\sim 0.5$  eV. The product ions are extracted from the ion source by a penetrating electric field and accelerated

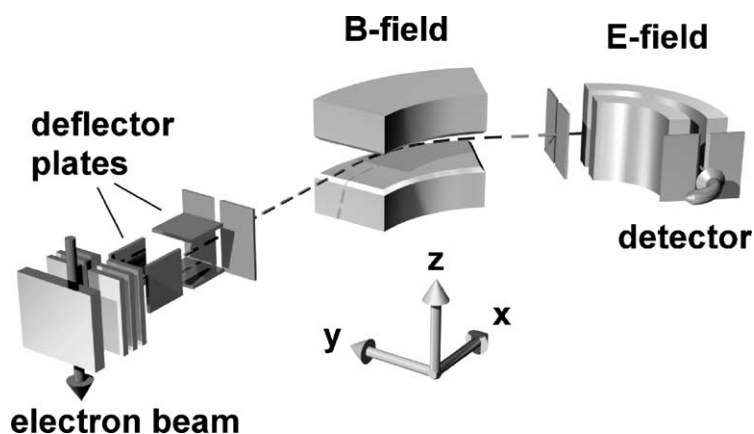


Fig. 1. Schematic view of the experimental setup. The two pairs of parallel plates for deflection of the ion beam perpendicularly to the beam direction are designated as deflector plates.

to 3 kV. Before entering the analyzing part of the mass spectrometer through a narrow entrance slit, the ions pass two pairs of perpendicular deflection plates that allow in principle a steering of the ion beam. For cross section measurements, these deflection plates are used to sweep the totally extracted ion beam across the entrance slit [40] and integrating the detected ion signal. In all other modes of operation, the deflection plates are not used to sweep the ion beam across the mass spectrometer entrance slit but are kept at fixed voltages and are only used for minor corrections of the ion trajectories to maximize the ion flux into the mass spectrometer. After passing through a magnetic sector-field followed by an electric sector-field, the ions are detected by a secondary electron multiplier operated in a counting mode. The combined action of the two sector-fields in a double focusing mass spectrometer results in a focusing of the ions within the plane of the instrument that accounts for angular and spatial spreads of the starting points of the ions and for small variations in the kinetic energy. However, the only way to compensate a velocity component outside of the plane of the instrument ( $z$ -direction, see Fig. 1) are the so called  $z$ -deflector plates right after the ion source. The ion yield measured as a function of the  $z$ -deflection voltage allows, in addition, to integrating the ion current over the  $z$ -direction (see above) the determination of the ki-

netic energy distribution for a given fragment ion [6,12].

### 3. Results

A mass spectrum of methane ionized by electrons of 100 eV kinetic energy is shown in Fig. 2. The electron current was set to 10  $\mu\text{A}$  and the methane pressure in the ion source was  $6 \times 10^{-5}$  Pa. Ions originating from the residual gas in the background ( $9 \times 10^{-7}$  Pa) were subtracted by a mass spectrum that has been measured without methane in the inlet system. The mass spectrum has not been corrected for discrimination effects due to initial kinetic energies of fragment ions and thus the peak heights do not correlate with the cross section values for this electron energy. The electron impact ionization cross sections and kinetic energy distributions for all ions that are labeled in the mass spectrum were determined in this study. At a mass per charge ratio of 3 and 6, the  $\text{H}_3^+$  and  $\text{C}^{2+}$  ions can be identified, however, the ion intensity for these ions is too low for further analysis. It is interesting to note that the relative ion yield for  $\text{H}_3^+$  and  $\text{C}^{2+}$  normalized to the  $\text{CH}_4^+$  parent ion agrees well with the corresponding values published by Ben-Itzhak et al. [28] for proton impact ionization at a projectile energy of 4 MeV.

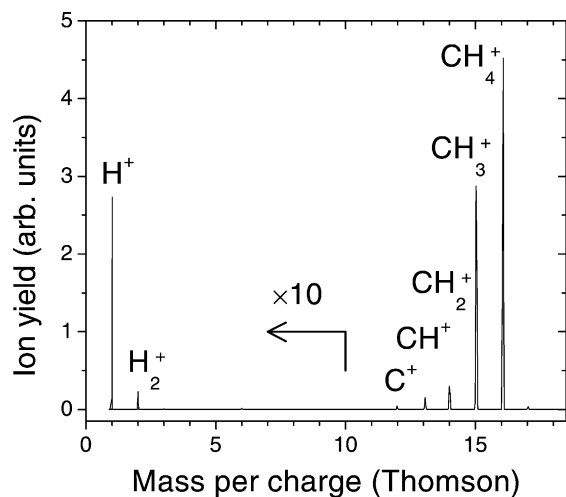


Fig. 2. Positive ion mass spectrum of  $\text{CH}_4$  ionized by 100 eV electrons and 10  $\mu\text{A}$  electron current. The pressure in the ion source was  $6 \times 10^{-5}$  Pa and the gas was thermalized at a temperature of 500 K. Please note that the ion signal for mass per charge ratios smaller than 10 Thomson was multiplied with a factor 10. This mass spectrum has not been corrected for reduced ion extraction and detection efficiency.

Figs. 3–6 show ion beam profiles in the  $z$ -direction for the parent ion  $\text{CH}_4^+$  and the fragment ions  $\text{CH}_2^+$ ,  $\text{C}^+$ , and  $\text{H}^+$  measured at different electron energies from the respective threshold to 800 eV. From these curves ion kinetic energy distributions were derived and a few examples are shown besides the  $z$ -profile diagrams. For this, in principle, the first derivative of the  $z$ -profile has to be plotted as a function of the square of the  $z$ -deflection voltage and multiplied by a factor that is determined by the geometry of the deflector plates and the acceleration voltage of the mass spectrometer (for details, see Ref. [6]). For a comparison, the diagrams that exhibit the kinetic energy distributions of  $\text{CH}_4^+$  and  $\text{CH}_2^+$  include the corresponding data of  $\text{Ar}^+$ . The kinetic energy of the  $\text{CH}_4^+$  ion is only determined by the ion source temperature that was 520 K throughout the present investigations. There is a surprising difference between the  $\text{Ar}^+$  and the  $\text{CH}_4^+$  parent ion that can be explained by two reasons: (i) Ar was introduced as a narrow collimated gas jet and thus the temperature of the neutral atoms was much colder than 520 K and (ii) the fragment ion  $^{13}\text{CH}_3^+$  will contribute

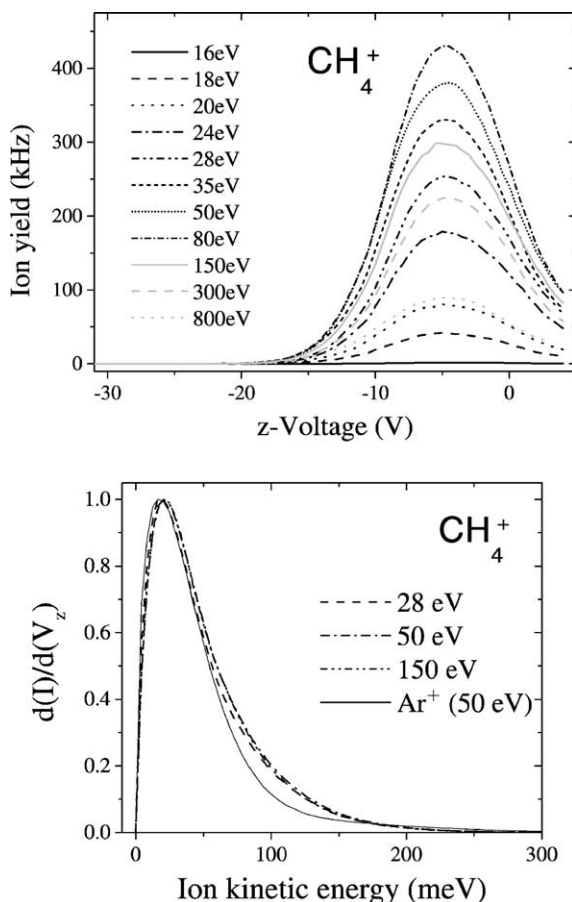


Fig. 3. The upper panel shows the ion beam profile of the  $\text{CH}_4^+$  parent ion in the  $z$ -direction. The ion signal was measured as a function of the voltage on the  $z$ -deflector pair. Different line styles designate different electron energies ranging from 16 to 800 eV, respectively. In the lower panel, the initial ion kinetic energy distributions were calculated from these  $z$ -profiles for three electron energies and compared to  $\text{Ar}^+$  that has been ionized from a cold gas jet. The ion kinetic energy distribution of  $\text{CH}_4^+$  shows no dependence on the electron energy.

by  $\sim 1\%$  to the  $^{12}\text{CH}_4^+$  ion signal. This fragment ion has the same mass per charge ratio as the  $\text{CH}_4^+$  parent ion but has a higher average kinetic energy than a parent ion. The difference between  $\text{Ar}^+$  and  $\text{CH}_4^+$  is 1.3 meV (average value of all electron energies) and increases from 0.5 meV for electron energies below 30 eV to 1.7 meV for electron energies larger than 30 eV. In contrast to the parent ion (Fig. 3) and the

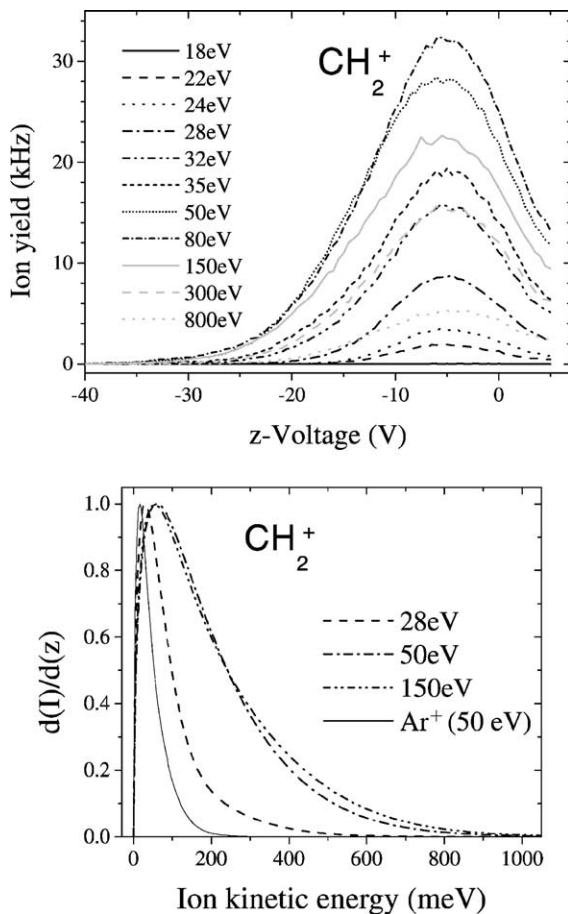


Fig. 4. The upper panel shows the ion beam profile of the  $\text{CH}_2^+$  fragment ion in the  $z$ -direction. The ion signal was measured as a function of the voltage on the  $z$ -deflector pair. Different line styles designate different electron energies ranging from 18 to 800 eV, respectively. In the lower panel, the initial ion kinetic energy distributions were calculated from these  $z$ -profiles for three electron energies and compared to  $\text{Ar}^+$  that has been ionized from a cold gas jet. In contrast to the parent ion  $\text{CH}_4^+$ , the width of the ion kinetic energy distribution increases dramatically by raising the electron energy from 28 to 50 eV, however, for higher electron energies the ion kinetic energy distribution remains practically constant.

$\text{CH}_3^+$ , the kinetic energy distribution of all other fragment ions reveals a pronounced dependence on the electron energy (Figs. 4–6), i.e., exhibiting wider distributions for higher electron energies. Furthermore, the  $z$ -profile deviate clearly from a single gaussian curve (Figs. 5 and 6) and thus the resulting kinetic

energy distribution will not be a Maxwell–Boltzmann type. For the  $\text{C}^+$  fragment ion, the kinetic energy distribution (Fig. 5) consists of two different contributions, a low one with an average kinetic energy of about 200 meV and a high energy part with an average value of about 400 meV. The relative height of the two distributions changes with the energy of the ionizing electron and this leads to the observed dependence of the average ion kinetic energy on the electron energy.

For the  $\text{H}^+$  fragment ion, kinetic energies exceeding 5 eV are found and the ion energy distribution reveals also two distinct contributions. According to ion trajectory calculations, ions with such high initial kinetic energies into the  $z$ -direction will be displaced roughly 4 mm from the beam axis when they reach the  $z$ -deflector. In order to pass the narrow tube through the magnetic sector-field these ions have to be deflected that much towards the center of the beam, otherwise they will not pass the defining slit after the electric sector-field. The present experimental setup starts to loose ions being deflected into the  $z$ -direction at initial kinetic energies larger than 2 eV. Thus, only ions starting into the direction of the mass spectrometer ( $x$ -direction) will be transmitted. Fiegele et al. [16] demonstrated recently the possibility of ion kinetic energy analysis with a sector-field mass spectrometer applying a retarding field method. The same experimental setup that was used in [16] has been applied for the ion kinetic energy analysis of the fragment ions from methane for  $\text{C}^+$  and  $\text{H}^+$  the results are shown in Figs. 5 and 6, respectively. For  $\text{C}^+$ , the agreement between the retarding field method and the  $z$ -profile analysis is very good, however, the high energy peak of the  $\text{H}^+$ , resulting from a dissociation of a doubly charged precursor ion cannot be observed by the  $z$ -deflection method due to discrimination effects discussed above.

Latimer et al. [13] determined in their synchrotron study the kinetic energy of the  $\text{H}^+$  fragment as a function of the photon energy in the range between 12 and 60 eV. Their energy spectra of fragment protons and deuterons exhibit three different contributions. The low energy part starts below the  $(2a_1)^{-1}$  threshold at 22.4 eV and indicates the existence of autoionizing Rydberg states which converge to the A state from

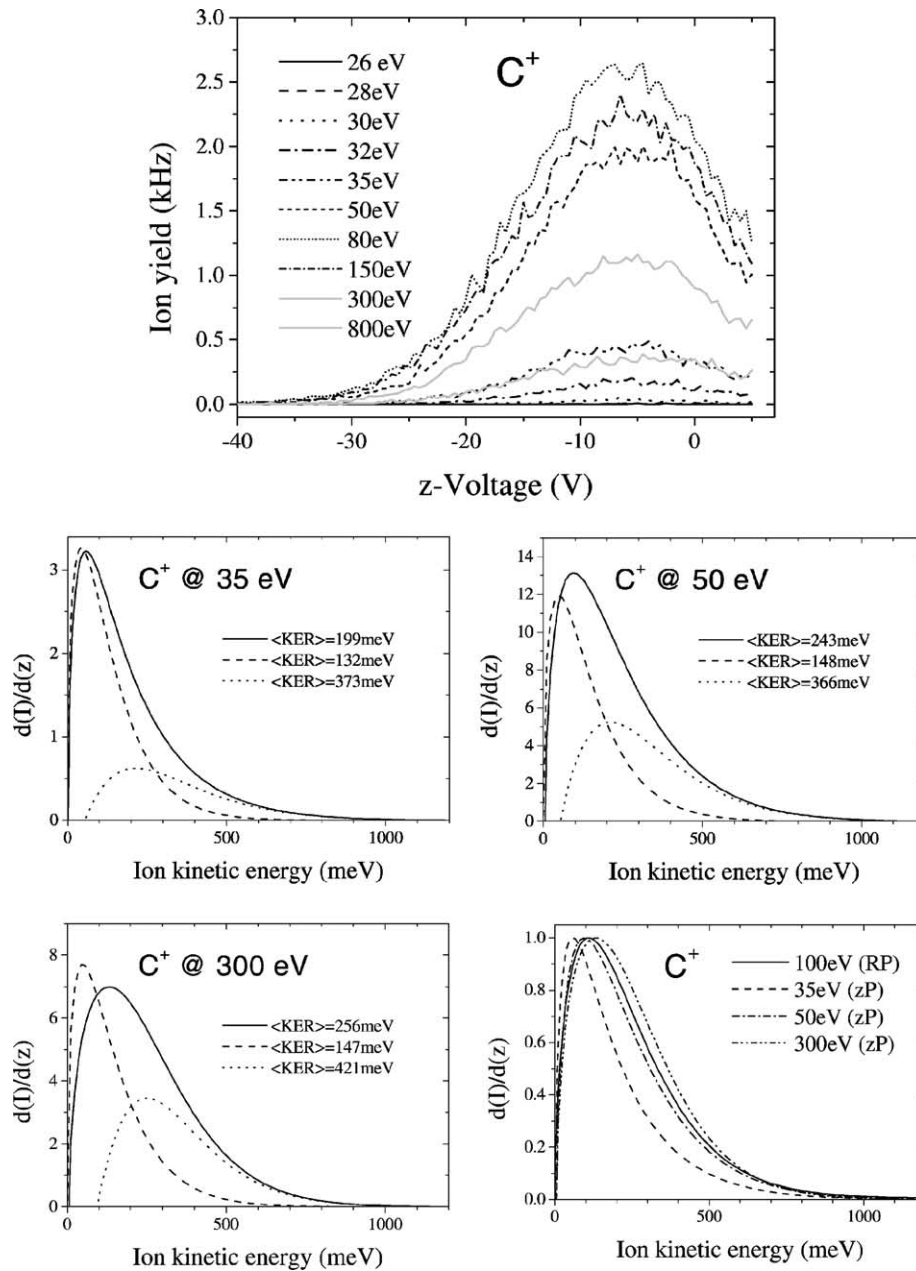


Fig. 5. The upper panel shows the ion beam profile of the  $C^+$  fragment ion in the  $z$ -direction. The ion signal was measured as a function of the voltage on the  $z$ -deflector pair. Different line styles designate different electron energies ranging from 26 to 800 eV, respectively. In three of the lower four panels, the initial ion kinetic energy distributions were calculated from these  $z$ -profiles for three electron energies (i.e., 35, 50, and 300 eV, respectively). The total ion kinetic energy distribution can be split into two parts (Maxwell–Boltzmann distributions) that have average energies of  $\sim 150$  and 400 meV. With increasing electron energy, the relative abundance of the two contributions changes in favor of the high energy part and thus the overall average kinetic energy shifts to higher values. The last (lower right) panel shows the overall ion kinetic energy distributions determined by the  $z$ -deflection method (ZP) in comparison to an ion kinetic energy distribution that was determined applying a retarding field technique (RP) (see text).

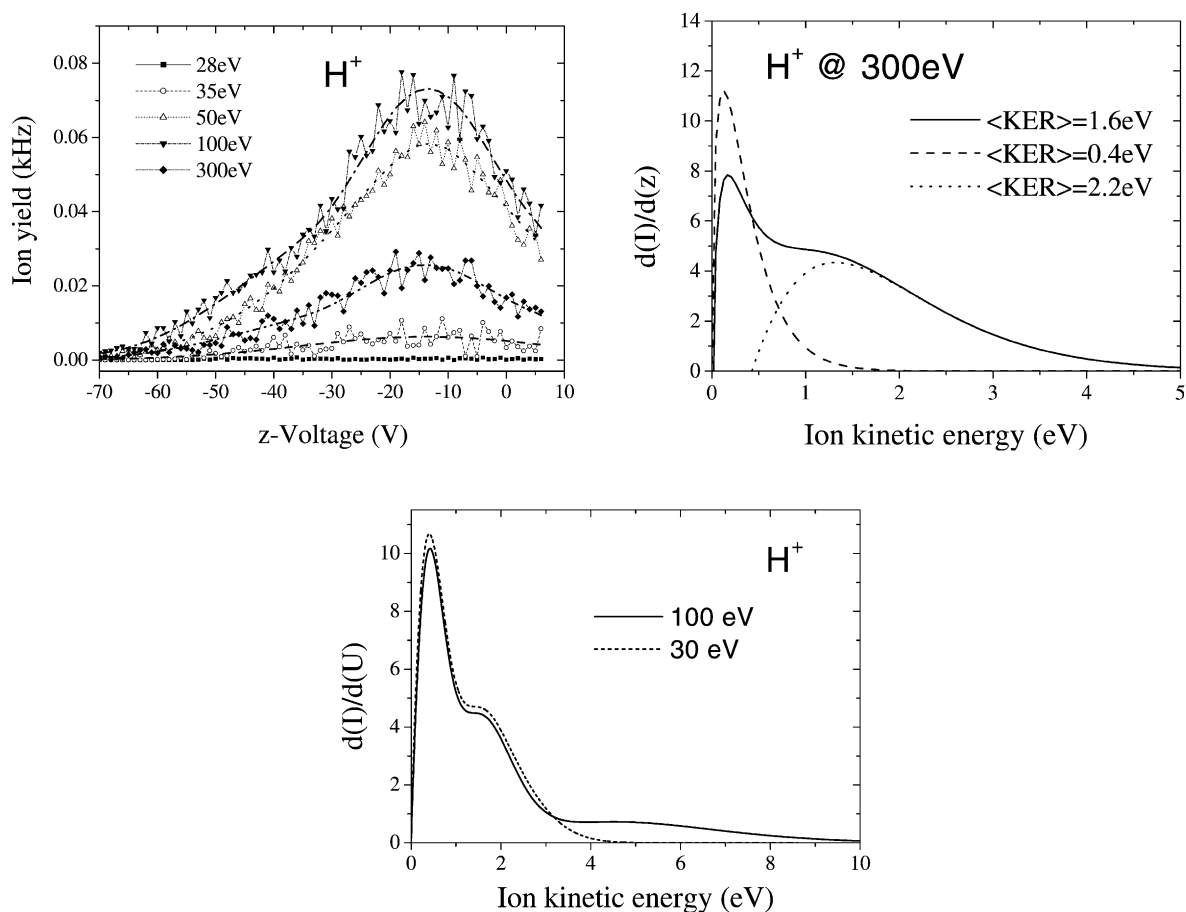


Fig. 6. The upper left panel shows the ion beam profile of the  $H^+$  fragment ion in the  $z$ -direction. The ion signal was measured as a function of the voltage on the  $z$ -deflector pair. Different line styles designate different electron energies ranging from 28 to 300 eV, respectively. In the upper right panel, the initial ion kinetic energy distribution was calculated from the  $z$ -profiles at an electron energy of 300 eV. The total ion kinetic energy distribution (solid line) clearly consists of two parts that are shown as dashed and dotted lines. The lower panel, finally shows the ion kinetic energy distributions of  $H^+$  determined with a retarding potential method at two electron energies. At electron energies higher than 30 eV, an additional high energy contribution can be observed that could not be detected with the  $z$ -profile technique due to discrimination effects (see text).

below. These Rydberg states have been observed previously in the production of excited H atoms by electron impact [41]. At photon energies higher than 26.6 eV, all the  $(2a_1)^{-1}$  states are accessible and the fragment protons and deuterons appear with a group of energies centered at 2.2 eV. In electron impact experiments, a similar group with an energy around 2.35 eV has been observed [15]. Finally, at photon energies higher than 35 eV, the threshold for double photoionization [42], Latimer et al. [13] detected an additional group of

protons having an average kinetic energy of 3.7 eV. This energy, however, turns out to be much smaller than the average kinetic energy of  $H^+$  from ion pair formation obtained by proton impact [28] or another photo-dissociation study by Fournier et al. [43] ending up with a value of about 6 eV. Except for the high energy part exceeding 3 eV, the ion kinetic energy distribution of  $H^+$  determined with the retarding potential method agrees well with the results published by Latimer et al. [13]. A possible reason for the differences

at high kinetic energies could be a reduced ion detection efficiency of the experimental setup used in [13]. It is interesting to note that the third group consisting of these high energy ions in the present study has an average kinetic energy of about 6 eV which agrees well with the proton impact results of Ben-Itzhak et al. [28] and the photoionization study of Fournier et al. [43].

In the upper panel of Fig. 7, the kinetic energies of all product ions of methane ionized by electron impact are plotted as a function of the energy of the ionizing electron. A logarithmic scale of the y-axis was cho-

sen, since the values for  $H^+$  are more than an order of magnitude larger than those of the parent ion  $CH_4^+$ . Assuming that only one splitting of an excited ionized complex into two fragments is responsible for the main part of the kinetic energy of the detected fragment ion it is possible to calculate (see lower panel of Fig. 7) the total kinetic energy that has been released in the dissociation process (KER). Thus, for fragment ions like  $C^+$  or  $CH^+$  where the excited  $CH_4$  complex decays into more than two fragments the calculated KER value will be a lower limit of the total KER. For

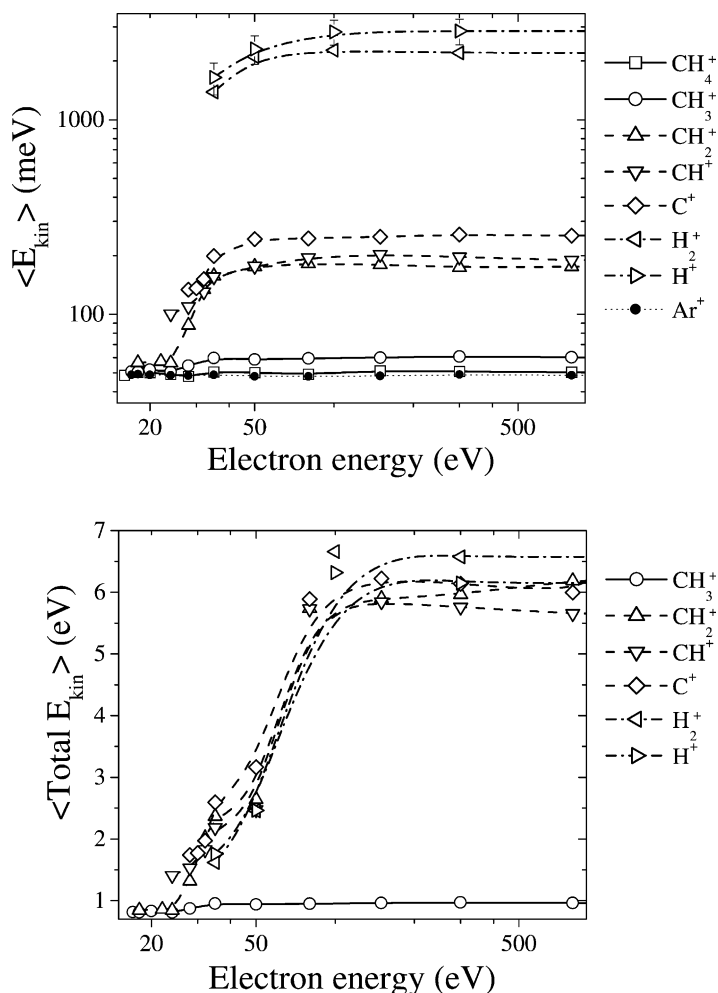


Fig. 7. Upper panel shows the average initial ion kinetic energy of methane product ions plotted as a function of the electron energy (logarithmic scale in both directions). Lower panel shows the average kinetic energy that has been released during the formation process of a given fragment ion assuming a splitting into two fragments (see text).

Table 1

Total average kinetic energy (in meV) released during the formation of fragment ions of methane at different electron energies

Electron energy (eV)	CH <sub>3</sub> <sup>+</sup>	CH <sub>2</sub> <sup>+</sup>	CH <sup>+</sup>	C <sup>+</sup>	H <sub>2</sub> <sup>+</sup>	H <sup>+</sup>
17	813	–	–	–	–	–
18	811	846	–	–	–	–
20	831	–	–	–	–	–
22	–	860	–	–	–	–
24	809	845	1406	–	–	–
26	–	–	–	–	–	–
28	872	1318	1530	1742	–	–
30	–	–	–	1772	–	–
32	–	2020	1826	1972	–	–
35	955	2367	2182	2591	1621	1759
50	937	2642	2473	3164	2459	2463
80	951	5736	5731	5888	–	–
100	–	–	–	–	6658	6317
150	961	5901	5845	6222	–	–
300	972	5966	5759	6137	6573	6148
800	962	6187	5654	5997	–	–

Splitting of a precursor ion into two parts was assumed using the most likely channels published by Ben-Itzhak et al. [28]. If the initial kinetic energy distribution of a channel consists of two or more energetic groups, only the part with the highest kinetic energy was used for this calculation.

H<sup>+</sup> and H<sub>2</sub><sup>+</sup>, the calculated KER does not depend strongly on the mass of the second fragment since the contribution of the heavy fragment to the KER is always small. However, in the case of C<sup>+</sup>, CH<sup>+</sup>, and CH<sub>2</sub><sup>+</sup>, the values of the total KER change almost by a factor of 2 if the second partner will have a mass of 1 Da (H or H<sup>+</sup>) or 2 Da (H<sub>2</sub> or H<sub>2</sub><sup>+</sup>). Table 1 lists the average total KER values for each fragment ion and electron energy where a *z*-profile was measured. If the energy distribution of an ion consists of two parts, the average kinetic energy of the high energy part was taken since ion pair formation by splitting of a doubly charged precursor can be expected. Except for the CH<sub>2</sub><sup>+</sup> where the probability for being formed together with an H<sub>2</sub><sup>+</sup> is quite high, all other carbon containing fragments are produced preferentially with H<sup>+</sup> as ion pairs [28]. The most likely channel according to Ben-Itzhak et al [28] was used for these total KER determination. The lower panel of Fig. 7 shows this total KER as a function of the electron energy. In contrast to the ion kinetic energies of the fragment ions shown in the upper panel, the total KER values for most of the fragment ions are very similar and lead to an average value of 6.1 eV for electron energies higher than 50 eV.

In previous investigations, it was pointed out that high kinetic energies of fragment ions have a strong influence on the ion collection efficiency and thus on resulting cross sections derived from ion efficiency curves [2,6–11]. Poll et al. [6] calculated discrimination factors for ions with different initial kinetic energies performing ion trajectory simulations of their ion source in a similar experimental setup as used here. These previous calculations neglected the presence of a magnetic field for guiding the electrons. The effect of this magnetic field having a field strength of about 40 mT can be neglected for all heavy ions, however, for H<sup>+</sup> and to a smaller degree also for H<sub>2</sub><sup>+</sup>, a substantial deflection of the ions into the *y*-direction was observed. Applying a newer version of SIMION [44], the extraction of the ions out of the Nier-type ion source was simulated with increased resolution of the potential array, for different mass per charge ratios and including the magnetic field. Furthermore, no approximations of planar or spherical geometry were made—the lenses were treated fully three-dimensional. Thereby, more reliable discrimination factors were derived. Fig. 8 shows the resulting correction factors for H<sup>+</sup> derived from the present

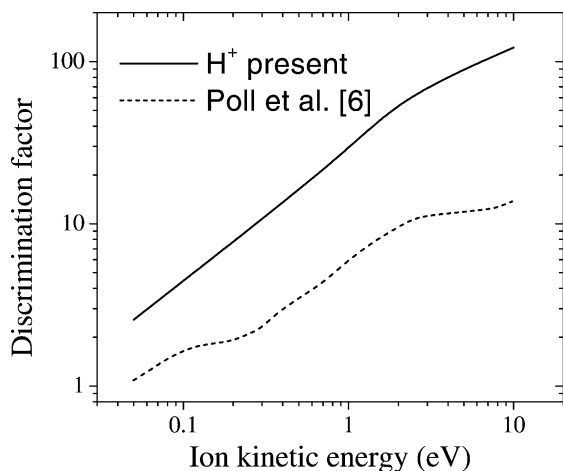


Fig. 8. Discrimination factor as a function of the initial kinetic energy of a fragment ion obtained by ion trajectory simulations. The ion source and the electrostatic lenses were treated fully three-dimensional. The dashed line represents the discrimination factors that were derived by Poll et al. [6] by treating the lenses as infinitely long slits.

simulations, including a magnetic field of 37 mT in the center part of the ion source, in comparison to the values published by Poll et al. [6]. Moreover, in contrast to Ref. [6] where constant discrimination factors were used for correction, the electron energy dependence of the  $z$ -profiles in the present study allows to

determine and use electron energy dependent discrimination factors. In addition, the present discrimination factors were determined using the complete kinetic energy distributions and not only the first momentum of the curve. Thereby, a more reliable cross section value can be obtained since the correction factor is not a linear function of the kinetic energy (see Fig. 8). In Fig. 9, the discrimination factors that have to be used to correct for reduced detection efficiency due to the initial kinetic energy of the ions are plotted as a function of the electron energy.

Multiplying the mass selected ion signal at each electron energy with the corresponding discrimination factors, the resulting ion signal will be proportional to the relative partial cross section. Adding up all ion signals, the resulting sum is proportional (with the same factor) to the total electron impact ionization cross section. At an electron energy of 100 eV, we determined this calibration factor (summation method, see [2]) by normalizing our relative total cross section to the absolute total cross section of Rapp and Englander-Golden [45]. Using this same normalization factor, absolute partial cross sections for all product ions, except  $\text{H}_3^+$  and  $\text{C}^{2+}$ , were derived and are shown in Fig. 10. For comparison, the diagrams in Fig. 10 also include some of the previously

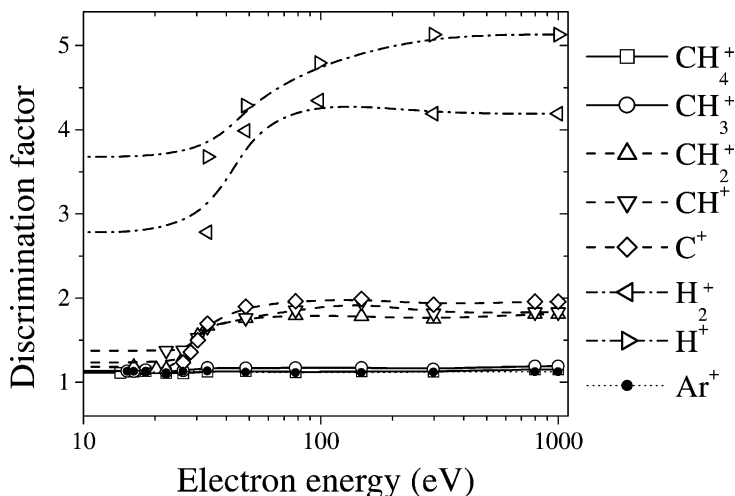


Fig. 9. Discrimination factors for each product ion plotted as a function of the electron energy. The factor was derived by calculation of the first momentum of the product of the ion kinetic energy distribution and the discrimination factor shown in Fig. 8.

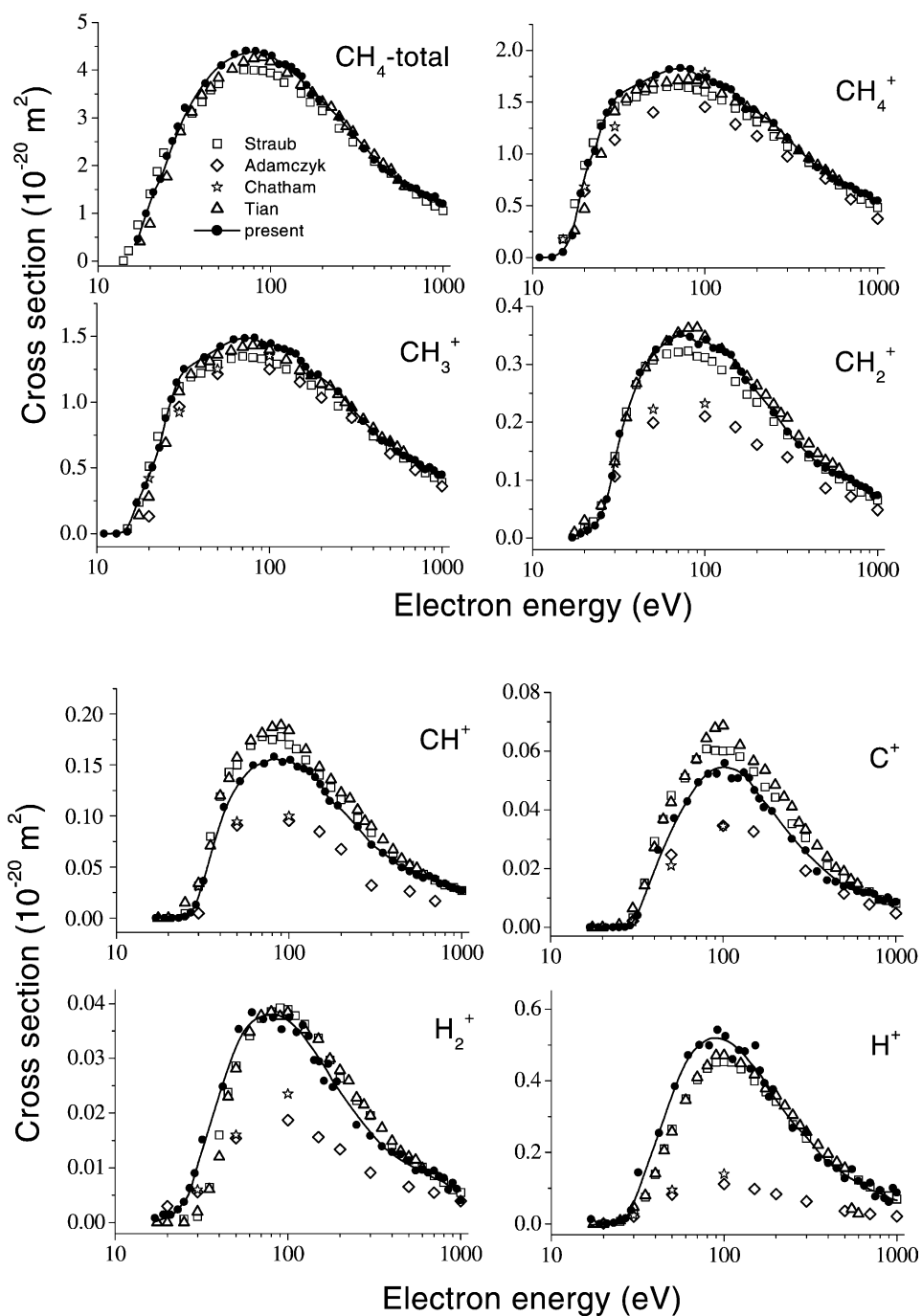


Fig. 10. Absolute partial cross sections for the formation of product ions by electron impact ionization of  $\text{CH}_4$ . The present values (filled symbols and line) are compared with data from the literature. There is good agreement with two experiments where complete ion detection was demonstrated (open square: Straub et al. [7]; open triangle: Tian and Vidal [8]).

published partial cross sections for  $\text{CH}_4$  product ions formed by electron impact. The agreement with the data determined with specially designed instruments for complete ion collection efficiency [7,8] is for all ions reasonably well. In contrast the values by Adamczyk et al. [9] and Chatham et al. [20] are for all fragment ions except  $\text{CH}_3^+$  significantly smaller than the present data and the results by [7,8]. In the case of  $\text{H}^+$ , the data differ by a factor of 5. The perfect agreement with the partial cross sections that were performed with instruments that were specially designed for cross section measurements for fragment ions that have initial kinetic energies larger than 5 eV clearly demonstrates the success of the present correction method. Furthermore, this work clearly demonstrates that commercial instruments can be applied for the determination of partial ionization cross sections. In contrast to the studies by Stebbings and coworkers [7] and Tian and Vidal [8], the present method especially in combination with the retarding potential method gives in addition the ion kinetic energy distribution of the fragment ions. In Fig. 11, as an example differential (with respect to the ion kinetic energy) partial cross sections for the formation of  $\text{CH}_2^+$  are shown. The upper figure shows cross sections close to the threshold region in a logarithmic scale and in the lower diagram the total cross section was split into kinetic energies above and below 120 meV (linear scale).

Latimer et al. [13] published partial cross sections for the formation of  $\text{H}^+$  by photoionization of methane for ions that were formed with kinetic energies exceeding a certain threshold value. It turns out that  $\text{H}^+$  was formed with kinetic energies exceeding 3.1 eV are produced only at photon energies larger than 35 eV. In following up this study, we measured here ionization efficiency curves close to threshold at two different retarding potentials, i.e., at the maximum of the  $\text{H}^+$  kinetic energy distribution and at a 5 V higher potential. As in the case of photoionization [13], the  $\text{H}^+$  ions that were formed with high kinetic energies (>5 eV) have a higher ionization energy than the low energy protons (see Fig. 12). The two lines drawn through the data in Fig. 12 correspond to fits using a Wannier type threshold law for electron impact ionization to the data (for

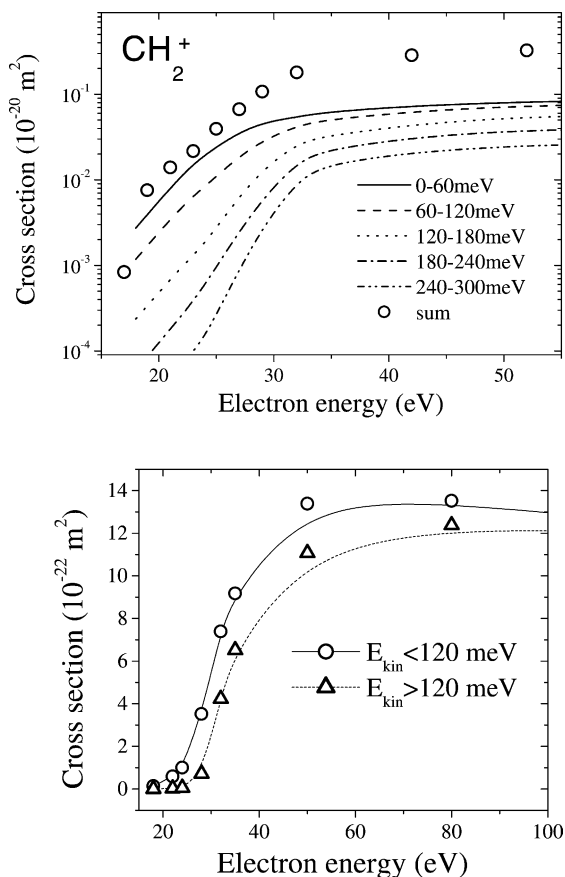


Fig. 11. Absolute partial electron impact ionization cross sections differential with respect to the initial ion kinetic energy of the  $\text{CH}_2^+$  fragment ion.

details of this fitting method, see [46,47]). According to the present data, the ionization energy for the fast  $\text{H}^+$  fragments is  $\sim 33$  eV whereas the threshold for  $\text{H}^+$  formation with low kinetic energies is  $\sim 26$  eV. The electron energy scale was calibrated with the ionization energy of  $\text{Ar}^+$  and  $\text{Ar}^{2+}$ . The present thresholds are in good accordance with what is known from photoionization, i.e., 26.6 eV is the threshold energy for photoionization of the  $(2a_1)^{-1}$  state [13] and 35 eV is the threshold for double photoionization [42] of  $\text{CH}_4$ .

The present study on  $\text{CH}_4$  was intended as an exploratory study to test the reliability of the methods used and developed in our laboratory. The agreement with the recent investigations by Straub et al. [7] and

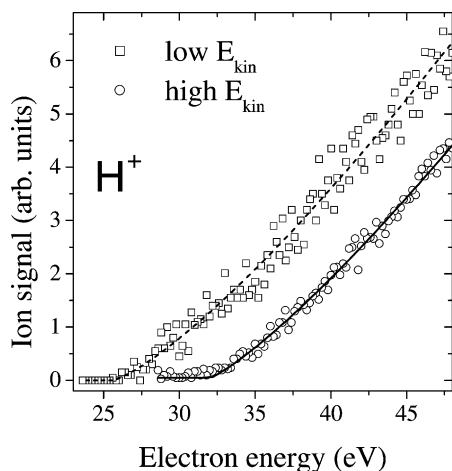


Fig. 12. Ion efficiency curves for  $H^+$  measured for two retarding potentials. For high retarding potentials, only protons that were formed with kinetic energies higher than 5 eV reach the detector (open circles). The lines through the data are a fit according to Wannier's threshold law [46,47].

Tian and Vidal [8] performed with instruments that were specially designed for partial cross section measurements clearly demonstrates that it is possible to correct ion efficiency curves measured with a standard instrument for reduced ion collection efficiency. Furthermore, the initial kinetic energy distribution for all product ions are measured with two different methods, i.e.,  $z$ -deflection and retarding potential. Due to different processes (ion pair formation or fragmentation of a singly charged precursor ion), the ion kinetic energy distribution of some fragment ions consists of more than one group, each group may have a quite different ionization threshold. The present experimental setup enables us also to determine partial cross sections that are differential according to the initial kinetic energy of the ion when it is formed. After this successful test for methane measurements with more complex hydrocarbon molecules in particular of relevance to plasma physics and chemistry are planned.

### Acknowledgements

This work was partially supported by the FWF, ÖNB, and ÖAW, Wien, Austria and the European

Commission, Brussels. This work has been carried out within the Association EURATOM-ÖAW. The content of the publication is the sole responsibility of the authors and does not necessarily represent the views of the EU Commission or its services.

### References

- [1] L.G. Christophorou (Ed.), *Electron Molecule Interactions and Their Applications*, Academic Press, Orlando, FL, 1984.
- [2] T.D. Märk, G.H. Dunn (Eds.), *Electron Impact Ionization*, Springer, Wien, 1985.
- [3] L.C. Pitchford, B.V. McKoy, A. Chutjian, S. Trajmar (Eds.), *Swarm Studies and Inelastic Electron-Molecule Collisions*, Springer, New York, 1987.
- [4] R.K. Janev (Ed.), *Atomic and Molecular Processes in Fusion Edge Plasmas*, Plenum Press, New York, 1995.
- [5] J.P. Mohr, W.L. Wiese (Eds.), *Atomic and Molecular Data and their Applications*, AIP Conference Proceedings, vol. 434, AIP, Woodbury, NY, 1998.
- [6] H.U. Poll, V. Grill, S. Matt, N. Abramzon, K. Becker, P. Scheier, T.D. Märk, *Int. J. Mass Spectrom. Ion Processes* 177 (1998) 143.
- [7] H.C. Straub, D. Lin, B.G. Lindsay, K.A. Smith, R.F. Stebbings, *J. Chem. Phys.* 106 (1997) 4430.
- [8] C. Tian, C.R. Vidal, *J. Phys. B: At. Mol. Opt. Phys.* 31 (1998) 895.
- [9] B. Adamczyk, A.J.H. Boerboom, B.L. Kistemaker, *J. Chem. Phys.* 44 (1966) 4640.
- [10] H.C. Straub, P. Renault, B.G. Lindsay, K.A. Smith, R.F. Stebbings, *Phys. Rev. A* 52 (1995) 1115.
- [11] C. Tian, C.R. Vidal, *J. Chem. Phys.* 108 (1998) 927.
- [12] R. Fuchs, R. Taubert, *Z. Naturforsch.* 19a (1964) 494.
- [13] C.J. Latimer, R.A. Mackie, A.M. Sands, N. Kouchi, K.F. Dunn, *J. Phys. B: At. Mol. Opt. Phys.* 32 (1999) 2667.
- [14] J. Apell, C. Kubach, *Chem. Phys. Lett.* 11 (1971) 486.
- [15] R. Loch, J.L. Olivier, J. Momigny, *Chem. Phys.* 43 (1979) 425.
- [16] T. Fiegele, C. Mair, P. Scheier, K. Becker, T.D. Märk, *Int. J. Mass Spectrom.* 207 (2001) 145.
- [17] K. Kameta, N. Kouchi, M. Ukai, Y. Hatano, *J. Electron Spectrosc. Relat. Phenom.* 123 (2002) 225.
- [18] J.A.R. Samson, G.N. Haddad, T. Masuoka, P.N. Pareek, D.A.L. Kilcoyne, *J. Chem. Phys.* 90 (1989) 6925.
- [19] G. Dujardin, D. Winkoun, S. Leach, *Phys. Rev. A* 31 (1985) 3027.
- [20] H. Chatham, D. Hills, R. Robertson, A. Gallagher, *J. Chem. Phys.* 81 (1984) 1770.
- [21] O.J. Orient, S.K. Srivastava, *J. Phys. B: At. Mol. Phys.* 20 (1987) 3923.
- [22] E. Krishnakumar, S.K. Srivastava, *J. Phys. B: At. Mol. Opt. Phys.* 23 (1990) 1893.
- [23] C. Vallance, S.A. Harris, J.E. Hudson, P.W. Harland, *J. Phys. B: At. Mol. Opt. Phys.* 30 (1997) 2465.

- [24] H.C. Straub, D. Lin, B.G. Lindsay, K.A. Smith, R.F. Stebbings, *J. Chem. Phys.* 106 (1997) 4430.
- [25] N. Duric, I. Cadez, M. Kurepa, *Int. J. Mass Spectrom. Ion Processes* 108 (1991) R1.
- [26] R. Fuchs, R. Taubert, *Z. Naturforschg.* 19a (1964) 1181.
- [27] M.D. Burrow, S.R. Ryan, W.E. Lamb Jr., L.C. McIntyre Jr., *J. Chem. Phys.* 71 (1979) 4931.
- [28] I. Ben-Itzhak, K.D. Carnes, D.T. Johnson, P.J. Norris, O.L. Weaver, *Phys. Rev. A* 49 (1994) 881.
- [29] V. Tarnovsky, A. Levin, H. Deutsch, K. Becker, *J. Phys. B: At. Mol. Opt. Phys.* 29 (1996) 139.
- [30] K.K. Irikura, Y.K. Kim, M.A. Ali, *J. Res. Nat. Inst. Stand. Tech.* 107 (2002) 63.
- [31] H. Deutsch, K. Becker, S. Matt, T.D. Märk, *Int. J. Mass Spectrom.* 197 (2000) 37.
- [32] S.P. Khare, M.K. Sharma, S. Tomar, *J. Phys. B: At. Mol. Opt. Phys.* 32 (1999) 3147.
- [33] V. Dose, P. Pecher, R. Preuss, *J. Phys. Chem. Ref. Data* 29 (2000) 1157.
- [34] M.E. Galassi, R.D. Rivarola, M. Beuve, G.H. Olivera, P.D. Fainstein, *Phys. Rev. A* 62 (2000) 022701.
- [35] K.N. Joshipura, M. Vinodkumar, U.M. Patel, *J. Phys. B: At. Mol. Opt. Phys.* 34 (2001) 509.
- [36] R. Stockbauer, *Int. J. Mass Spectrom. Ion Phys.* 25 (1977) 401.
- [37] R. Taubert, *Adv. Mass Spectrom.* 1 (1959) 489.
- [38] H.E. Stanton, J.E. Monahan, *J. Chem. Phys.* 41 (1964) 3694.
- [39] H.U. Poll, C. Winkler, D. Margreiter, V. Grill, T.D. Märk, *Int. J. Mass Spectrom. Ion Processes* 112 (1992) 1.
- [40] V. Grill, G. Walder, P. Scheier, M. Kurdel, T.D. Märk, *Int. J. Mass Spectrom. Ion Processes* 129 (1993) 31.
- [41] C.Y.R. Wu, D.L. Judge, *J. Chem. Phys.* 75 (1981) 172.
- [42] P.A. Hatherly, M. Stankiewicz, L.J. Frasinski, K. Codling, *Chem. Phys. Lett.* 159 (1989) 355.
- [43] P.G. Fournier, J. Fournier, F. Salama, P.J. Richardson, J.H.D. Eland, *J. Chem. Phys.* 83 (1985) 241.
- [44] David A. Dahl, SIMION 6.0, Idaho National Engineering and environmental Laboratory.
- [45] D. Rapp, P. Englander-Golden, *J. Chem. Phys.* 43 (1965) 1464.
- [46] T. Fiegele, G. Hanel, I. Torres, M. Lezius, T.D. Märk, *J. Phys. B* 33 (2000) 4263.
- [47] G. Hanel, B. Gstir, T. Fiegele, F. Hagelberg, K. Becker, P. Scheier, A. Snegursky, T.D. Märk, *J. Chem. Phys.* 116 (2002) 2456.